J. Fluid Mech. (1978), *vol.* 88, *part* 1, *pp.* 71–96
Printed in Great Britain

Instability and transition of the axisymmetric wake of a slender body of revolution

By LEIGH F. PETERSON† AND FRANCIS R. HAMA

Department of Aerospace and Mechanical Sciences, Princeton University, Princeton, New Jersey 08540

(Received 1 July 1977 and in revised form 2 March 1978)

The growth of small disturbances in the incompressible axisymmetric wake of a slender body of revolution has been studied experimentally. The experiments were performed in a running water channel at a Reynolds number of 3600 based on the body diameter and free-stream velocity, without any artificial stimulation of the wake. Digital techniques have been used to analyse the output signals of a multichannel hot-film anemometer system.

Analysis of the mean velocity profiles and the velocity fluctuations shows that the wake can be divided into three regimes: the near wake or adjustment region, a region of locally parallel flow, and the far wake. The near wake is characterized by the adjustment of the mean velocity profile from that in the boundary layer of the body to the wake profile. At the same time, the structure of the disturbances in the boundary layer seems to adjust to a different structure in the wake. Large velocity gradients in both the streamwise and the radial direction are present in this region. In the region of locally parallel flow, a helical mode disturbance is superseded by a mode which appears to be mostly a planar oscillation of higher frequency and amplification rate. Higher-order harmonics of dominant frequency components have been identified in these experiments. The far wake is the region in which nonlinear interactions appear to predominate. The experimental measurements and hydrogen bubble photographs indicate the presence of large scale transverse disturbances in this region, associated with roll-up of the fluid.

1. Introduction

Transition from laminar to turbulent flow has been the subject of extensive research and debate since the latter part of the nineteenth century. Schubauer & Skramstad (1947) published the first systematic experimental analysis of the stability of a given flow configuration. Their examination of small disturbances induced in the laminar boundary layer on a flat plate, coupled with Lin's (1944, 1945) improvements of the Tollmien–Schlichting theory, yielded excellent agreement between experimental measurements and the neutral stability curve. The stability of small disturbances in a compressible boundary layer was investigated experimentally by Laufer & Vrebalovich (1960) and Kendall (1975), and from a theoretical point of view by Mack (1969). The problem of a two-dimensional jet has been studied by Tatsumi &

† Present address: Research School of Physical Sciences, The Australian National University, P.O. Box 4, Canberra A.C.T. 2600.

Kakutani (1958), Curle (1957), Sato (1959) and Michalke (1965), whilst Sato & Kuriki (1961), and Mattingly & Criminale (1972) give experimental results and stability theories for the two-dimensional wake.

The axisymmetric jet has also received considerable attention. Theoretical analyses have been given by Batchelor & Gill (1962), Mattingly & Chang (1974), and more recently Morris (1976).

The experimental investigations of the jet include Viilu (1962), Reynolds (1962) and Freymuth (1966). Sato & Okada (1966) give an analysis and experimental results for the stability of small disturbances in an axisymmetric wake, and Lessen & Singh (1973) give a more extensive analysis of axisymmetric shear flows.

The experimental investigation of the stability of the axisymmetric wake by Sato & Okada was performed on a wake in which artificial stimulation of the small disturbances was used to ensure reproducible transition. Such artificial stimulation of small disturbances may seem to be a reasonable way of testing their stability, however it is equally possible that the excitation may completely overwhelm the mechanism of natural transition. Unlike the vibrating ribbon used by Schubauer & Skramstad, which induces an effectively localized disturbance in the boundary layer, the disturbances in the Sato–Okada experiment were introduced by a loudspeaker. As Schubauer & Skramstad reported, the loudspeaker would establish a certain pressure field which might undesirably control the instability process. It therefore comes as no surprise that substantial differences between artificially induced and natural transition of a two-dimensional wake have been discovered lately by Sato & Saito (1975). It is reasonable to assume that similar differences would occur in the axisymmetric case.

We describe an experimental investigation of the instability and natural transition of the axisymmetric wake behind a slender streamlined body of revolution with a needle-sharp trailing tip. Our earlier paper, Hama & Peterson (1976), describes an experimental investigation and semi-empirical analysis of the laminar wake behind the same body. In that case the Reynolds number was 2000. In the present case, with the body accurately aligned and a Reynolds number of 3600, preliminary observations of a dye streak injected into the boundary layer of the body and then swept downstream showed that within five body lengths of the trailing tip the wake exhibited several distinct flow regimes. A photograph of the body and dye streak in the water channel is shown in figure 1 (plate 1). Water flow is from left to right. As the downstream distance from the trailing tip is increased, the initially straight dye line develops some sort of varicose motion, and then becomes a confused cloud of diluted dye. The output signal of a hot-film anemometer probe showed that adjacent to the trailing tip of the body velocity fluctuations appeared to be quite smooth and low in amplitude. On the other hand, velocity fluctuations farther downstream possessed progressively larger amplitudes and eventually became quite violent in character. This paper, in which we have attempted to identify the structure and behaviour of the most unstable disturbance in a wake which undergoes natural transition, may be regarded as presenting the second step of our long range plan to investigate thoroughly phenomena in axisymmetric wakes.

2. Stability theory of axisymmetric free shear layers

The linearized stability theory for axisymmetric free shear layers has been developed by several authors. For the linearized theory, disturbance quantities are written in cylindrical polar co-ordinates (x, y, ϕ), as

$$u^* = Re\,[F(y)\exp\{in\phi + i\alpha(x-ct)\}], \tag{1}$$

$$v^* = Re\,[H(y)\exp\{in\phi + i\alpha(x-ct)\}], \tag{2}$$

$$w^* = Re\,[iG(y)\exp\{in\phi + i\alpha(x-ct)\}], \tag{3}$$

$$p^* = Re\,[P(y)\exp\{in\phi + i\alpha(x-ct)\}], \tag{4}$$

where $F(y)$, $H(y)$, $G(y)$, $P(y)$ are complex amplitude functions, c is the wave velocity and α is the axial wavenumber. The azimuthal wavenumber n defines the periodicity of the fluctuations with respect to the azimuthal co-ordinate ϕ. With fluctuations of the type (1)–(4), the inviscid stability equation may be written in non-dimensional form as

$$(u-c)\frac{d}{dy}\left\{\frac{y}{n^2+\alpha^2y^2}\frac{d}{dy}(yG)\right\} - (u-c)\,G - yG\frac{d}{dy}\left(\frac{yu'}{n^2+\alpha^2y^2}\right) = 0. \tag{5}$$

The stability characteristics of three disturbance modes, each described by a different value of n, have been investigated from a theoretical point of view. These modes are: (i) When $n = 0$, the velocity fluctuation is axisymmetric, and the phase does not change in the azimuthal direction. (ii) When $n = 1$, the phase of the velocity fluctuation changes by 2π in one revolution around the axis. This represents the sinuous or helical mode. (iii) When $n = 2$, the phase changes by 4π in one revolution around the axis.

Batchelor & Gill obtained solutions of (5) with appropriate boundary conditions for the temporal analysis of an axisymmetric jet with a mean velocity profile

$$U(y) = U_0/(1+y^2/y_0^2)^2, \tag{6}$$

where U_0 is the mean velocity on the jet axis and y_0 is the jet half-width. They concluded that the $n = 0$ mode is stable and that velocity fluctuations of the sinuous mode $n = 1$ do amplify.

The temporal stability of the axisymmetric wake profile

$$u(y) = 1 - q\exp(-ay^2), \tag{7}$$

where q and a are constants used to express the mean velocity profile in non-dimensional form, has been investigated by Sato & Okada. Through numerical analysis of the stability of this profile to small perturbations, they found that the $n = 0$ mode is stable, whereas $n = 1$ is unstable. No solution could be obtained for the $n = 2$ mode.

Lessen & Singh give a stability analysis which includes the effect of viscosity up to Reynolds numbers near 200, in addition to the inviscid case, for both temporal and spatial stability analyses of the axisymmetric jet and wake profiles. Their detailed computations show that the $n = 0$ and $n = 2$ modes are stable, and the $n = 1$ mode is unstable in both configurations.

For the experiments described here the wake Reynolds number (based on centre-line velocity defect and half-wake radius) is approximately 500 at $x = 2$, and 400 at $x = 3$, and we assume that the stability analysis for the wake under study may be approximated by that applicable to small disturbances in an inviscid fluid.

3. Experiment

The experiments discussed in this paper were performed in the J. E. Nicholson tilting flume facility of the Hydrodynamics Laboratory, Princeton University, using the same experimental arrangement as described in our earlier paper (Hama & Peterson 1976; Peterson 1975). The slender body of rotation (30 cm long, 1·8 cm maximum diameter) used to generate the wake was suspended by fine tungsten wires and aligned with the mean velocity direction in the region of uniform channel flow. At a Reynolds number

$$R = Ud/\nu$$

(where d is the maximum body diameter and U is the free-stream velocity) of 3600, the free-stream turbulence level was less than 0·1 %. Throughout the experiments the Reynolds number for the suspension wires was less than 10, and vortex shedding from these wires was neither expected nor detected in the free-stream or wake of the body. Although very small velocity defects due to the wakes of the wires were observed near the body, these decayed rapidly with increasing downstream distance, and had no measurable effect on the wake of the axisymmetric body. At this higher Reynolds number no wobbling motion of the body could be detected from movement of a laser beam reflected from the body surface.

Velocity measurements were made using Thermo-Systems constant-temperature hot-film anemometer systems (model 1050A anemometer modules in conjunction with model 1057 signal conditioners and the model 1051–2 digital read-out for mean velocity measurements). Up to four different channels were used simultaneously depending on the flow parameters to be investigated. All probes were type 1210-20W. These probes are of conventional hot-wire type, fitted with a quartz-coated hot-film sensor 0·05 mm diameter and 1 mm long.

A cursory examination of the output signals from the anemometers showed the frequencies and fluctuations in the wake to be less than about 10 Hz. Digital analysis of the signals using a high speed computer was chosen as the most convenient technique for analysis of the fluctuations. Prior to digitizing, the signals were actively high pass filtered ($f_c = 0{\cdot}1$ Hz) to remove the d.c. component, and low pass filtered ($f_c = 15$ Hz) to minimize aliasing of higher frequency components. This filtered signal was subsequently amplified and recorded on an accurately calibrated instrumentation tape recorder (Hewlett Packard 3960A) operated in the FM mode. Later the recorded tapes were played back through low pass filters (to remove any extraneous high frequency tape noise) preceding a multichannel fast analog to digital conversion system (type DATACOM 810B) used to generate digital tapes for analysis on an IBM 360/91 computer. A typical recorded signal for one probe location consisted of one hundred blocks on the digital tape, each block containing 256 data points for each anemometer channel of interest. The sequences of filtered and amplified voltage signals were then numerically rescaled using the appropriate probe calibrations to

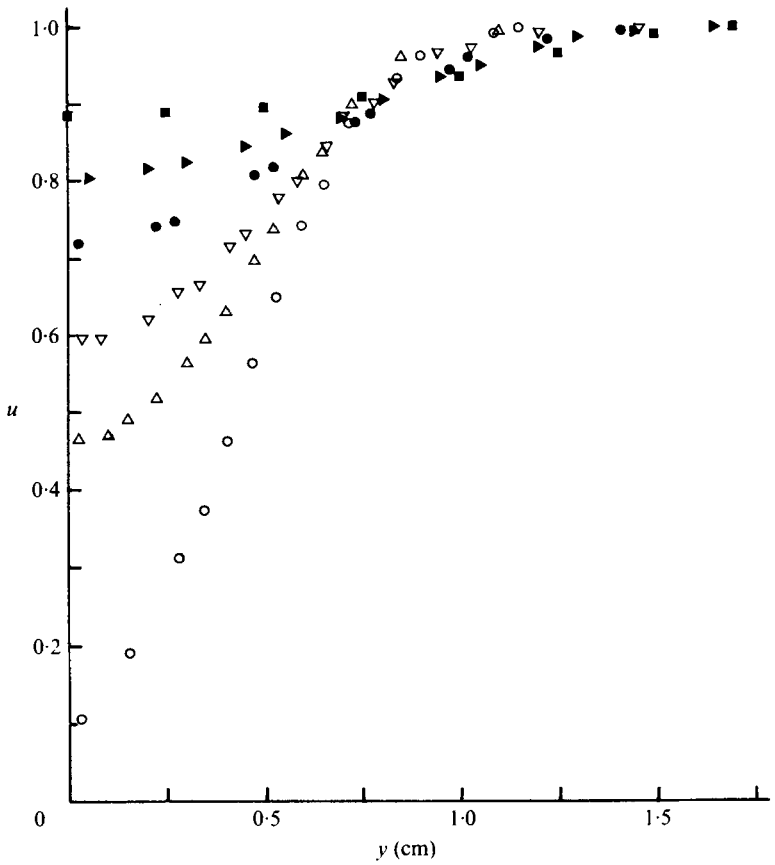

FIGURE 2. Mean velocity profiles of the wake. ○, $x = 0$; △, $x = 1{\cdot}0$; ▽, $x = 2{\cdot}0$; ●, $x = 3{\cdot}0$; ▶, $x = 4{\cdot}0$; ■, $x = 5{\cdot}0$.

give digital time series of the actual velocities detected by the sensors. Energy spectra and phase relationships of the signals were computed using the method of Stegen & Van Atta (1970).

4. Results

Non-dimensionalized velocity profiles for the locations $x = 0{\cdot}0$, $1{\cdot}0$, $2{\cdot}0$, $3{\cdot}0$, $4{\cdot}0$ and $5{\cdot}0$ where x is the distance downstream from the trailing tip of the body, expressed in terms of the body length, are shown in figure 2. Each profile was obtained after the minimum velocity point for a given downstream location had been found and the axisymmetry of the wake checked. Near the trailing tip of the body the central core of fluid contiguous to the wake axis is rapidly accelerated, with very little change apparent in the outer part of the wake. Farther downstream the profiles become much flatter and spread in the radial direction. Figure 3 shows the wake centre-line velocity u_c as a function of the downstream position x. The rapid acceleration of the fluid near the body is evidenced by the increases in wake centre-line velocity that take place in the region $x \leqslant 1{\cdot}0$. Downstream of $x = 1{\cdot}0$ however, the rate of increase in u_c

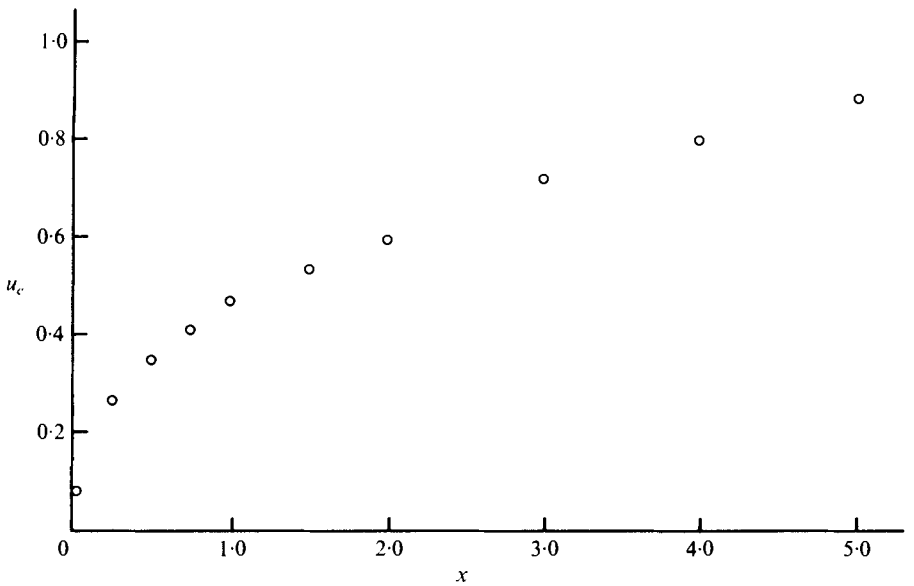

FIGURE 3. Centre-line velocity *vs.* downstream distance.
○, present experimental data.

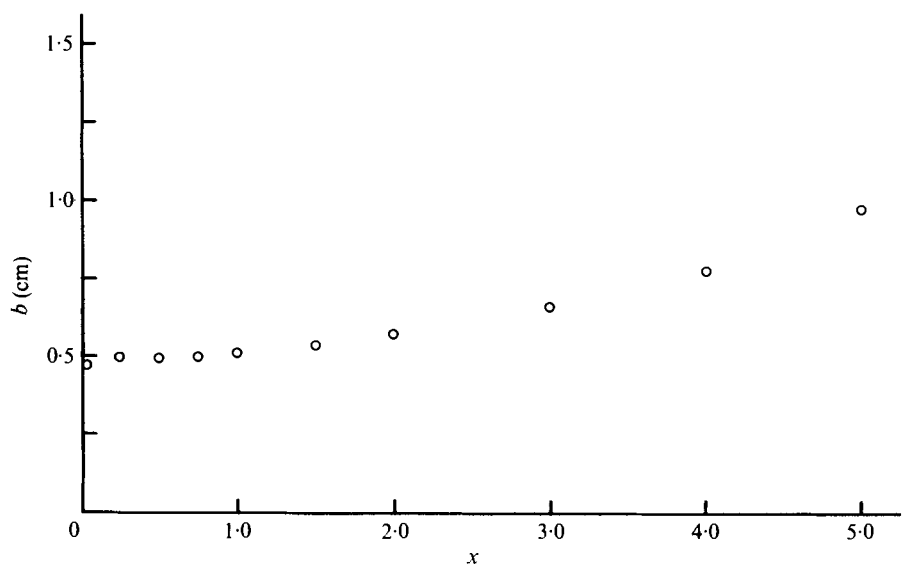

FIGURE 4. Half-wake radius *vs.* downstream distance. ○, present experimental data.

becomes less. In the far wake, at $x = 5{\cdot}0$, $u_c \simeq 0{\cdot}9$ and does not show the much more gradual increase observed in the laminar case.

The half-wake radius b is shown plotted against downstream distance in figure 4. At the trailing tip of the body there is a sudden increase in b, similar to that reported in our investigation of the laminar wake. Thereafter the half-wake radius increases very slowly, until about $x = 3{\cdot}5$. The large increases in b that take place in the region downstream of $x = 3{\cdot}5$ may be an indication that transition is taking place.

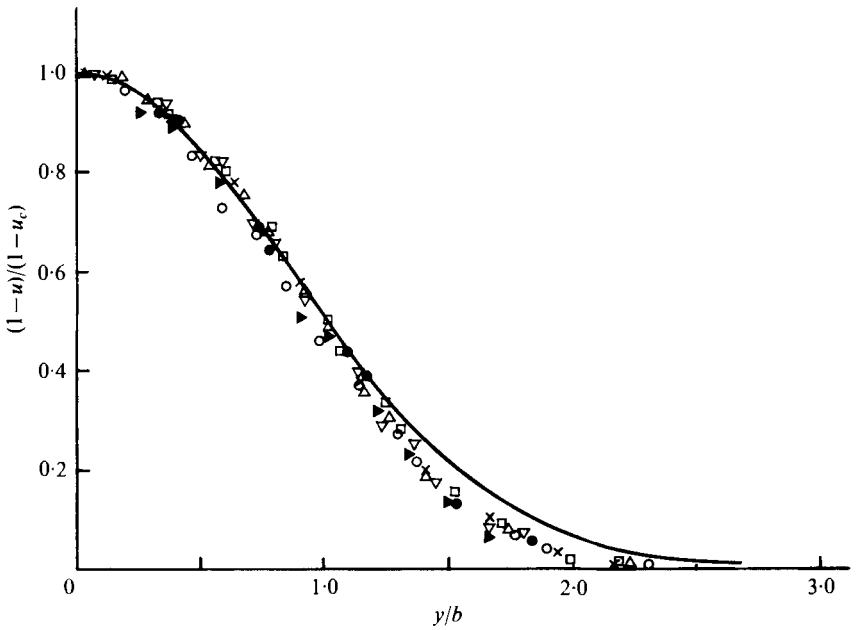

FIGURE 5. Non-dimensional velocity defect *vs.* normalized radial co-ordinate. ○, $x = 0$; ×, $x = 0{\cdot}5$; △, $x = 1{\cdot}0$; □, $x = 1{\cdot}5$; ▽, $x = 2{\cdot}0$; ●, $x = 3{\cdot}0$; ▶, $x = 4{\cdot}0$; ——, $\exp[-\ln 2(y/b)^2]$.

In figure 5 we show the normalized velocity defect $(1-u)/(1-u_c)$ versus the radial co-ordinate expressed in terms of the half-wake radius b. It is immediately apparent that the velocity defect profile exhibits some approximate geometrical similarity over the entire range of x locations at which measurements were made. For comparison the mean velocity defect profile of the asymptotic similarity solution for the axisymmetric wake

$$\frac{1-u}{1-u_c} = \exp\left\{-\ln 2\left(\frac{y}{b}\right)^2\right\}$$

(Rosenhead 1963) is included in this figure. This profile is assumed as the mean profile of the wake in the stability analyses of Sato & Okada (1966) and Lessen & Singh (1973). Near the wake axis this theoretical profile appears to describe the experimental results adequately, however, some discrepancy is apparent in the outer region of the wake. In terms of actual velocities the differences between the experimental results and this theoretical profile become progressively smaller with increasing x, owing to the corresponding decrease in centre-line velocity defect.

The longitudinal velocity fluctuations (u^*) were examined using a single hot-film probe with the cylindrical sensor perpendicular to the mean velocity component. Depending on the downstream position, the fluctuations appear to range from a more or less sinusoidal wave form to an eventual chaotic 'turbulence-like' signal.

The radial distribution of the overall r.m.s. value of u^* for various downstream locations is shown in figure 6. Near the trailing tip of the slender body the distribution is bimodal, with a centre-line amplitude comparable to the free-stream turbulence level. Between $x = 3{\cdot}0$ and $4{\cdot}0$, the r.m.s. distribution changes from the well developed

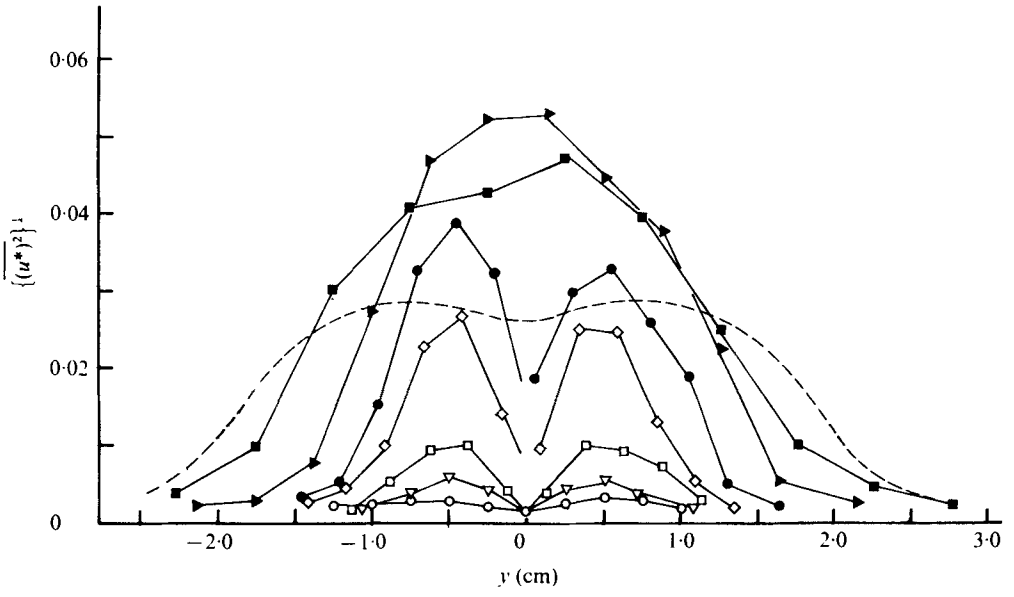

FIGURE 6. Amplitude distribution of overall longitudinal velocity fluctuations. ○, $x = 0$; ▽, $x = 0{\cdot}75$; □, $x = 1{\cdot}5$; ◇, $x = 2{\cdot}5$; ●, $x = 3{\cdot}0$; ▶, $x = 4{\cdot}0$; ■, $x = 5{\cdot}0$; – – –, Chevray.

bimodal profile to a profile for which the centre-line value is the peak amplitude. Downstream of this point the maximum r.m.s. value no longer increases with x, but rather tends to decrease. At the same time the fluctuations spread in the radial direction. This behaviour, coupled with the increase in b and u_c described previously, might be taken as an indication of the occurrence of transition. It is noteworthy that in the region where the distribution is bimodal, the peak amplitude of the fluctuations occurs near the radius where the mean velocity profile has an inflexion point.

Chevray (1968) examined the turbulent wake of a slender axisymmetric body. In his experiments the boundary layer on a six-to-one prolate spheroid, for which $Ud/\nu = 4{\cdot}6 \times 10^5$, was tripped to produce a turbulent boundary layer and wake. The results of his measurements of u^* at the farthest downstream location have been scaled by the parameters for our experiments and are shown, for comparison, in figure 6. The amplitude of fluctuations near the axis at $x = 5{\cdot}0$ in the present experiment is considerably larger than the amplitude of fluctuations observed in the decaying fully turbulent wake. On the other hand, the fluctuations in the turbulent wake are spread farther in the radial direction.

Representative energy spectra selected from spectra computed at approximately two hundred and fifty locations in the wake, together with a small portion of the appropriate anemometer signal are shown in figures 7–13. In figures 7–12 diagram (*a*) is the signal and energy spectrum obtained on the wake axis, whereas diagram (*b*) corresponds to those obtained at a radius where the peak amplitude occurs in the bimodal distribution. Figure 13 shows the signals and associated energy spectra at the outer edge of the wake far downstream of the slender body. Plotted energy spectra are not normalized, and the origin of the vertical scale is shifted according to the

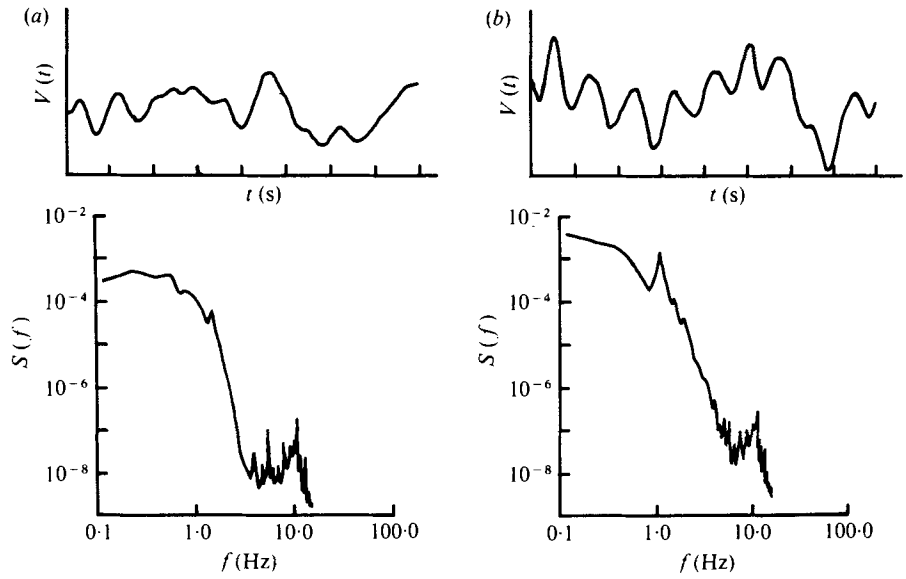

FIGURE 7. Signals and energy spectra at $x = 0$. (*a*) centre-line; (*b*) $y = 0{\cdot}5$ cm. $V(t)$ = anemometer output voltage, $S(f)$ = energy density at frequency f(cm^{2}s^{-1}).

magnitude of the signal. For all spectra $\Delta f = 0{\cdot}112$ Hz; no smoothing of spectra was employed. Careful analysis of the free-stream turbulence present under a variety of operating conditions in the flume showed that there was no unique fluctuation frequency dominant in its energy spectrum.

The main features of the signals and energy spectra in the wake are as follows: at the trailing tip of the body [$x = 0$, figure 7(*a*)] the increased sensitivity of the hot-film anemometer at low velocities effectively amplifies the small velocity fluctuations, yielding large voltage fluctuations. The energy spectrum does not show appreciably dominant peaks as would be obtained if strong sinusoidal components were present in the fluctuations. The sharp peaks at high frequencies in this energy spectrum result from the electronic noise of the anemometer system. The amplitude of this noise is not entirely negligible compared with the signals of interest at this location. Off the axis, at the maximum r.m.s. region [figure 7(*b*)] the fluctuating signal clearly shows a sinusoidal component to be present. This component yields a distinct spike in the energy spectrum at a frequency of approximately 1 Hz.

Figure 8 shows that at $x = 1{\cdot}0$, the signals and spectra are qualitatively the same as those observed at $x = 0$. In figure 8(*b*) the energy spectrum is again dominated by a sharp spike at a frequency of 1 Hz.

On the wake axis, at $x = 2$, the velocity fluctuations appear to show some regularity, however they are of small amplitude [figure 9(*a*)]. On the other hand, at the radius where the overall r.m.s. value has its maximum values the fluctuating signal and corresponding energy spectrum shown in figure 9(*b*) are quite different from those previously described. The fluctuations are now very regular, although the amplitude is not constant. Instead, signals of large amplitude occur in bursts for short periods of time, interspersed with smaller amplitude fluctuations of the same frequency. This intermittent appearance of larger signal amplitudes is similar to the observations by

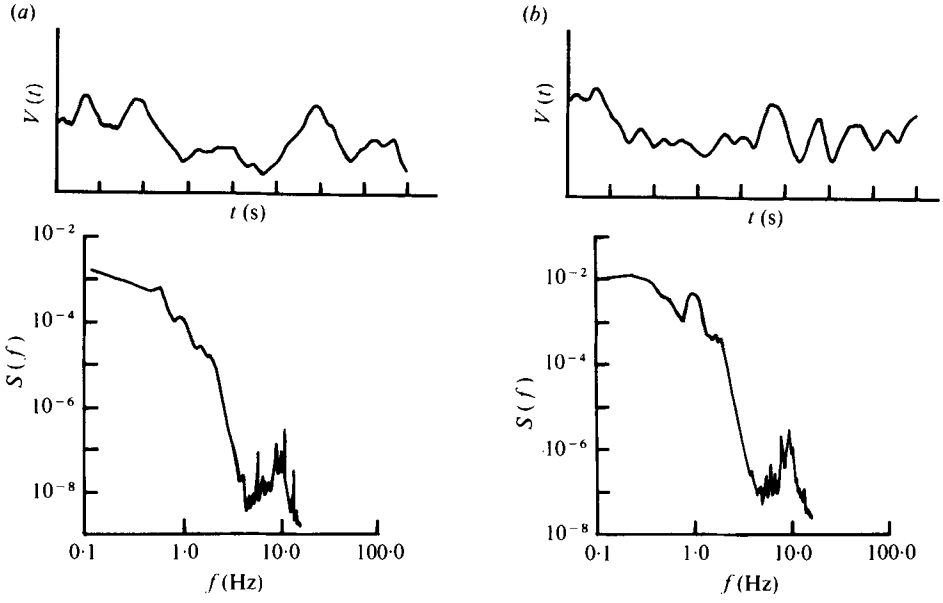

FIGURE 8. Signals and energy spectra at $x = 1{\cdot}0$. (*a*) Centre-line, (*b*) $y = 0{\cdot}5$ cm.

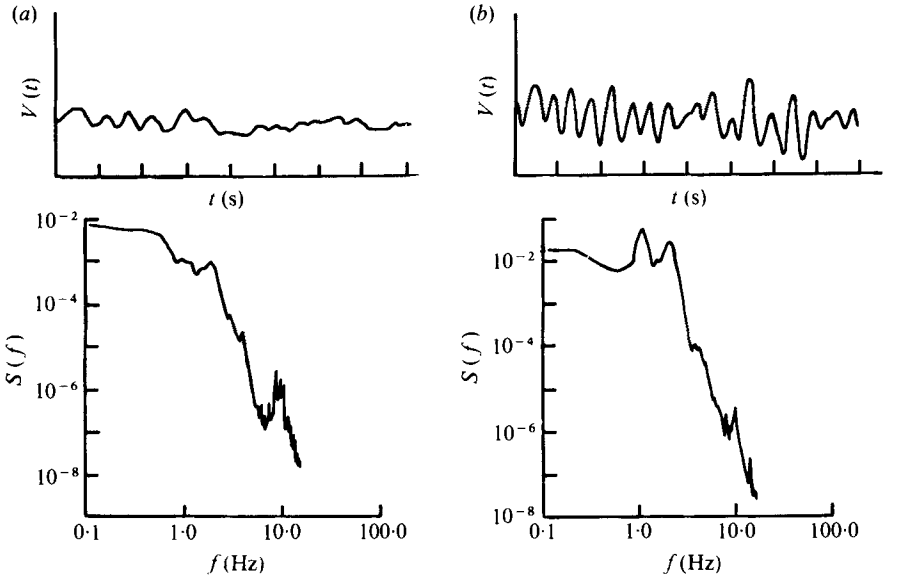

FIGURE 9. Signals and energy spectra at $x = 2{\cdot}0$. (*a*) Centre-line, (*b*) $y = 0{\cdot}5$ cm.

Schubauer & Skramstad in their experiments with the natural transition of a boundary layer. The energy spectrum indicates the presence of two distinct frequency components. One peak is at the same frequency as that previously observed (1·0 Hz). A second peak at approximately 2·0 Hz, which was barely discernible at the $x = 1{\cdot}0$ location, has developed an amplitude comparable to that at 1·0 Hz.

On the wake axis at $x = 3{\cdot}0$, 'bursts' of large amplitude velocity fluctuations

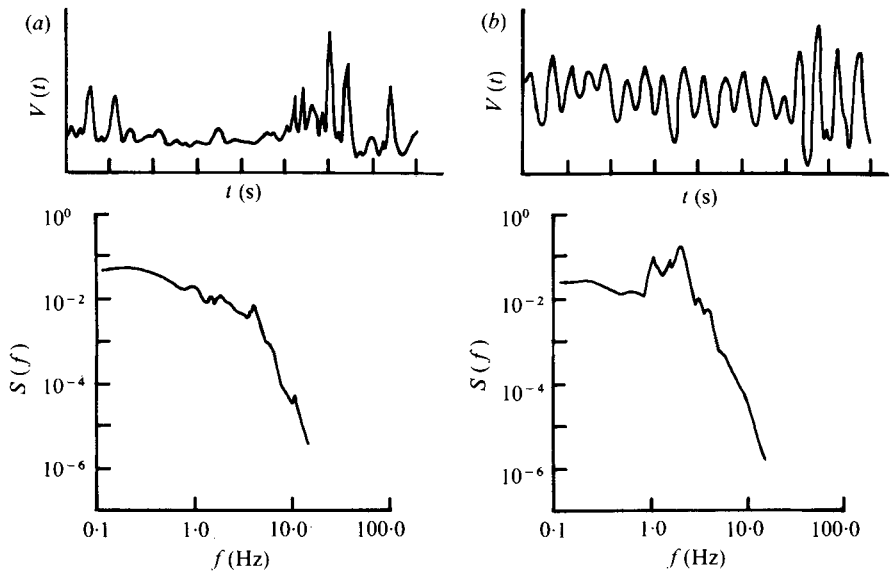

FIGURE 10. Signals and energy spectra at $x = 3{\cdot}0$. (*a*) Centre-line, (*b*) $y = 0{\cdot}5$ cm.

appear in an otherwise quiescent signal [figure 10(*a*)]. This burst, however, is different in nature from the slow amplitude modulation of a fixed frequency previously observed at off-axis locations. The burst here is such that large one-sided upward spikes, corresponding to increases in velocity, intermittently occur. In addition to the 1·0 and 2·0 Hz peaks in the energy spectrum, a peak at approximately 4·0 Hz is also present. Away from the wake axis [figure 10(*b*)] the fluctuations remain very regular, and show the same sort of slow amplitude modulation previously described at $x = 2{\cdot}0$. The energy spectrum shows that here 2·0 Hz is the dominant frequency component; its amplitude is much larger than that of the 1·0 Hz component.

The signals and spectra obtained at $x = 4$ are shown in figure 11. We recall that at about this x location the amplitude of the longitudinal velocity fluctuations increased to the maximum value and the bimodal distribution was destroyed. Figure 11(*a*) shows that on the wake axis large amplitude fluctuations, which still preserve a one-sided and intermittent nature, predominate in the signal. The energy spectrum shows the presence of large amplitude 2·0 and 4·0 Hz components. At a radius of 0·75 cm, some regularity is discernible in the velocity fluctuations, although regions of apparently random activity occur most of the time. The energy spectrum is dominated by a frequency component at slightly greater than 2 Hz.

At the farthest downstream location where measurements were made, $x = 5$, figure 12(*a*) shows a signal observed on the wake axis which is quite similar to those encountered in turbulent flows. The energy spectrum is smoother than those previously obtained on the wake axis, and the peak at approximately 2 Hz has become less prominent. Away from the axis, the signal still shows regularity at a predominant frequency of approximately 2 Hz. However, a certain randomness prevails in the signal, accompanied by indications of higher frequency breakdown at the extremities of large amplitude velocity fluctuations. It is worth noting that the energy density for $f = 10$ Hz at $x = 5{\cdot}0$ is approximately three orders of magnitude larger than it is at

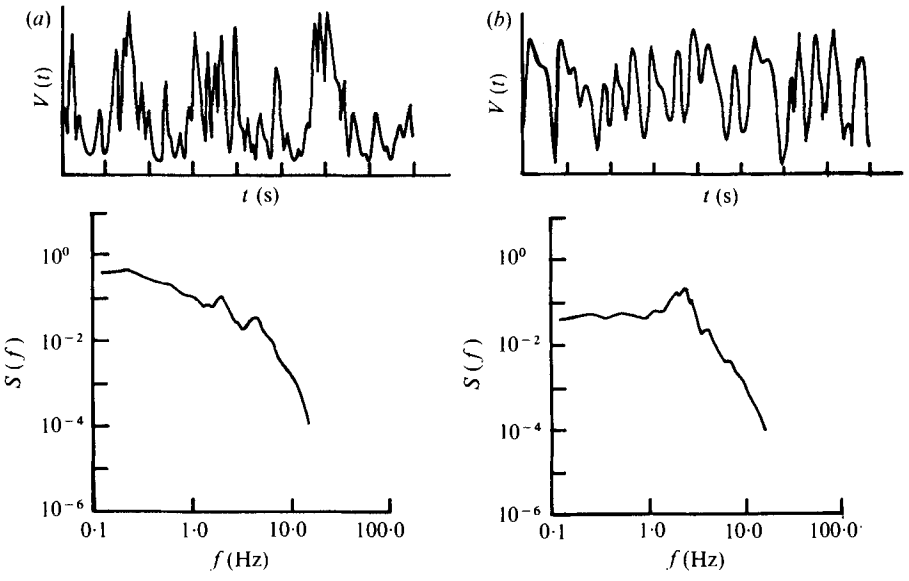

FIGURE 11. Signals and energy spectra at $x = 4{\cdot}0$. (*a*) Centre-line, (*b*) $y = 0{\cdot}75$ cm.

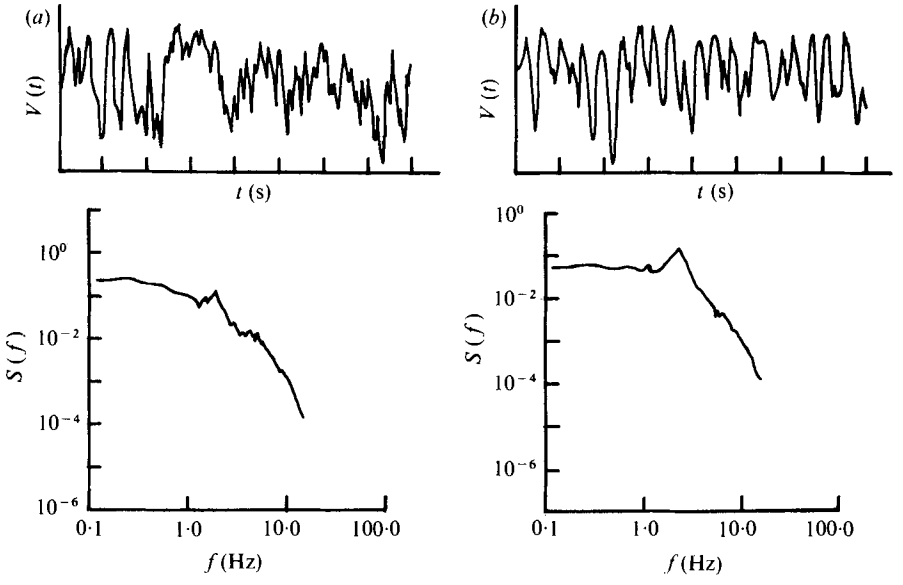

FIGURE 12. Signals and energy spectra at $x = 5{\cdot}0$. (*a*) Centre-line, (*b*) $y = 0{\cdot}8$ cm.

$x = 2{\cdot}0$. This is an indication of the 'broadening' of the energy spectrum that occurs far downstream of the body. In this far downstream region, $x \geqslant 4{\cdot}0$, the signals observed near the outer edge of the wake are quite unlike those anywhere else. Figures 13(*a*) and 13(*b*) show that sharp downward spikes, corresponding to decreases in velocity, occur at frequent intervals. For the remainder of the time, only small fluctuations are present. The energy spectra of both signals indicate the presence of a 2 Hz component, though less pronounced than in the preceding figures. Otherwise the

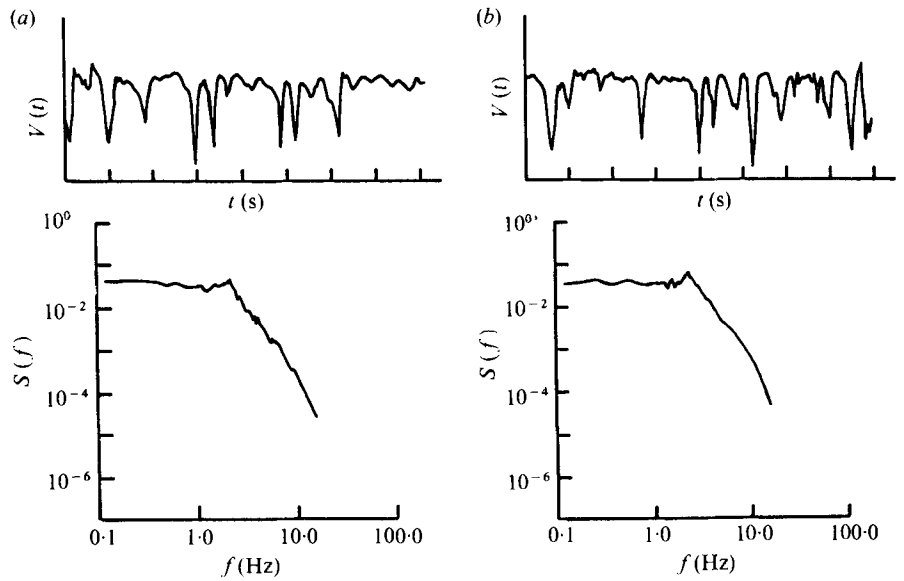

FIGURE 13. Signals and energy spectra at the outer edge of the wake. (*a*) $x = 4{\cdot}0$, $y = 1{\cdot}12$ cm. (*b*) $x = 5{\cdot}0$, $y = 1{\cdot}5$ cm.

spectra are quite smooth. This one-sidedness of the signals is an indication of outward burstings of lower momentum fluid from within the wake.

The radial distribution of the amplitude of the 1·0 Hz component is shown in figure 14. Qualitatively this exhibits the same behaviour as the overall r.m.s. distribution shown in figure 6. Initially the distribution is bimodal, and between $x = 3{\cdot}0$ and $x = 4{\cdot}0$, the centre-line amplitude increases to a value close to the maximum measured at that downstream position. It is not certain, however, whether the bimodal distribution ceases to exist, or the spacing of measurement points is too large to resolve the centre-line characteristics at these locations. It is quite possible that at such far downstream locations as these the general unsteadiness of the flow smears out such details. Between $x = 4{\cdot}0$ and $x = 5{\cdot}0$, there is some spreading in the radial direction.

Figure 15 shows that the 2·0 Hz component behaves in a similar manner, with the same apparent increase in centre-line amplitude at about $x = 4{\cdot}0$. Figures 14 and 15 show that the maximum amplitude of the 2·0 Hz component is 30–40% larger than the maximum amplitude of the 1·0 Hz component.

The streamwise behaviour of the peak values of (*a*) the overall r.m.s. value of longitudinal velocity fluctuations, (*b*) the 1·0 Hz component and (*c*) the 2·0 Hz component are shown in figure 16.

As was previously shown, an apparent maximum value in the overall fluctuations is attained at about $x = 3{\cdot}5$ or $x = 4{\cdot}0$. Further downstream the centre-line value (which is the peak value) appears to level off, and even tends to decrease. In the region $x \simeq 0{\cdot}5$ to $x \simeq 3{\cdot}0$, the amplitude of the 1·0 Hz component grows exponentially with increasing downstream distance. A straight line drawn through the data points, which are plotted using a logarithmic ordinate, yields a non-dimensional spatial amplification rate

$$-\alpha_i = 0{\cdot}0076$$

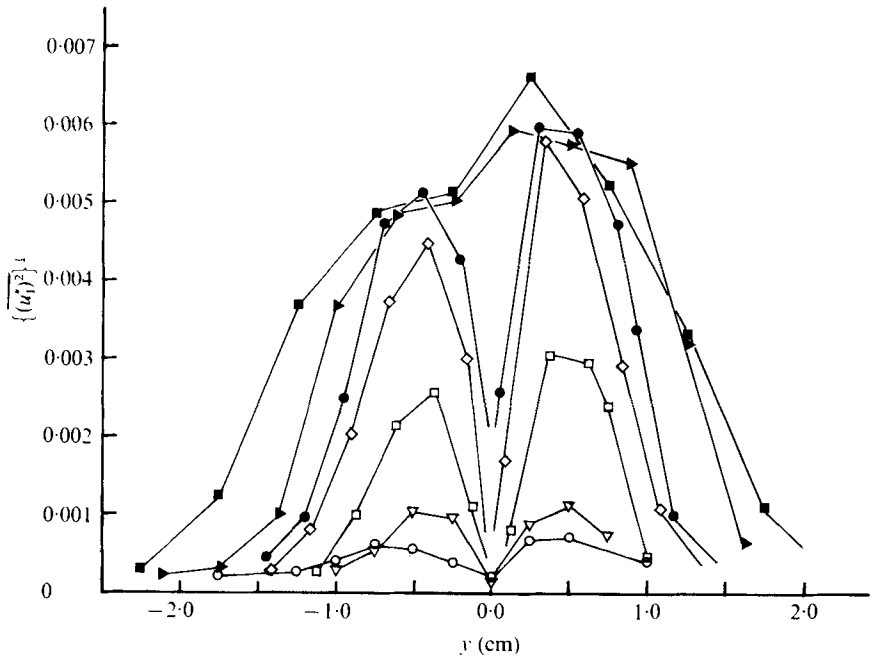

FIGURE 14. Amplitude distribution of the 1·0 Hz component of the longitudinal velocity fluctuations. For symbols see figure 6.

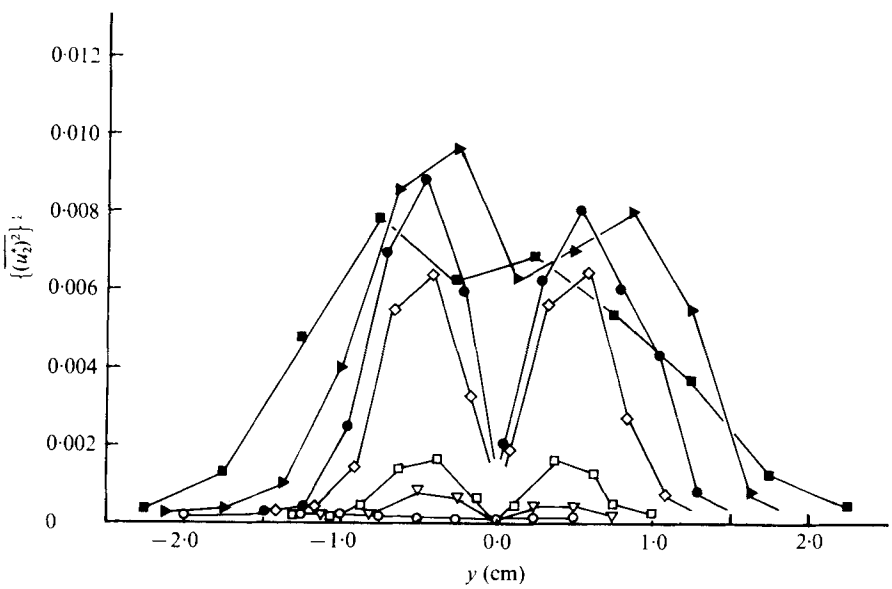

FIGURE 15. Amplitude distribution of the 2·0 Hz component of the longitudinal velocity fluctuations. For symbols see figure 6.

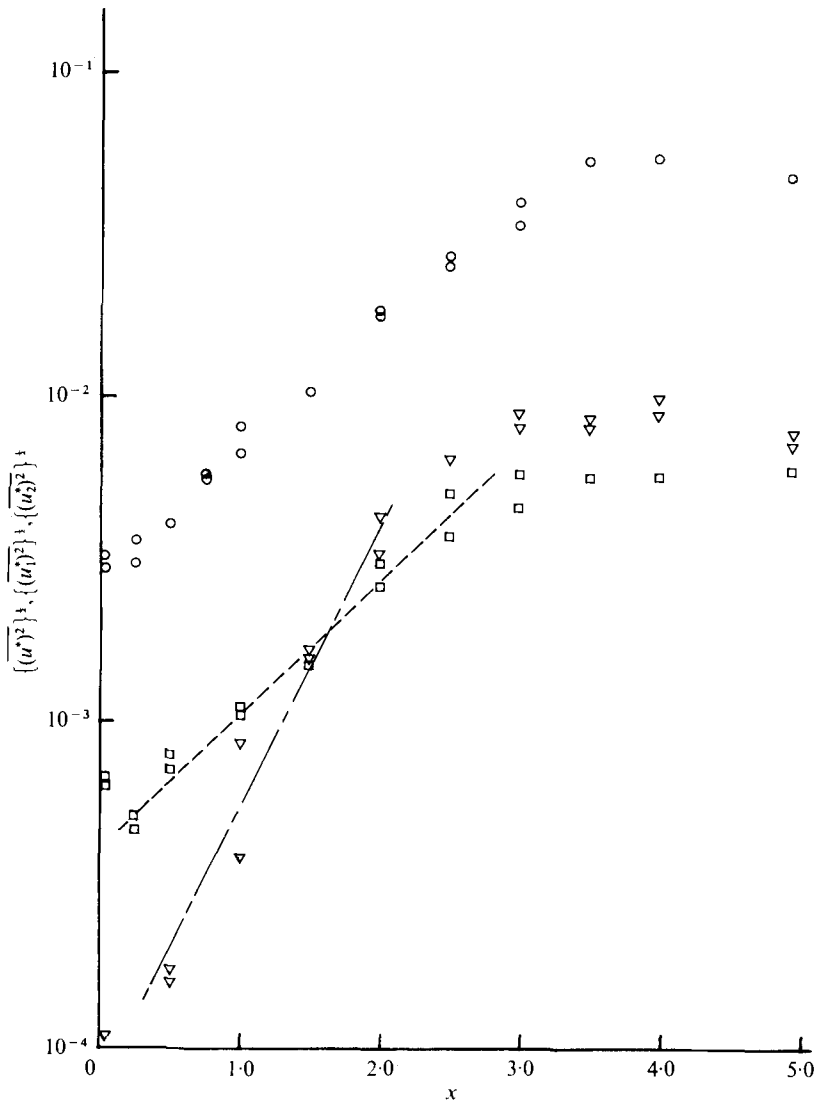

FIGURE 16. Streamwise behaviour of the peak amplitude of (*a*) ○, overall r.m.s. distribution of longitudinal velocity fluctuations; (*b*) □, 1·0 Hz component; (*c*) ▽, 2·0 Hz component.

for this component. Similar exponential growth is evident for the 2·0 Hz component, for which

$$-\alpha_i = 0{\cdot}0155.$$

Corresponding non-dimensional wavenumbers are 0·214 for the 1·0 Hz component, and 0·429 for the 2·0 Hz component. It is significant that both the 1·0 Hz and 2·0 Hz components coexist right from the early stages of the wake development, and that the 2·0 Hz component does not seem to be the result of nonlinear development of the 1·0 Hz component. While they are still in the linear amplification stages, the amplitude of the 2·0 Hz component, in fact, exceeds that of the 1·0 Hz component before both level off at about $x = 3{\cdot}0$.

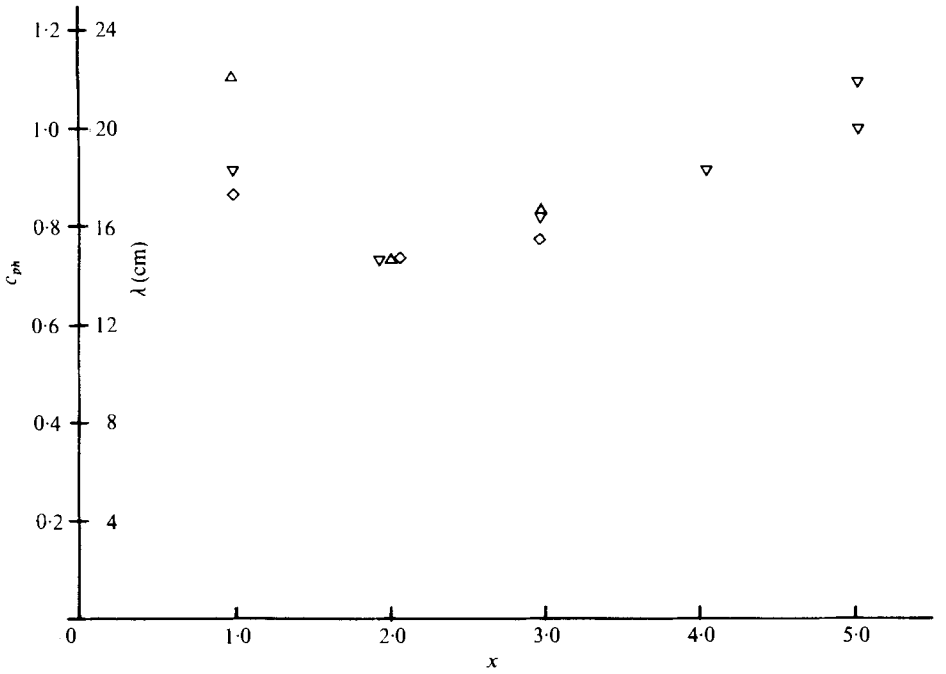

FIGURE 17. Wavelength and phase velocity of the 1·0 Hz component.
△, $y = 0{\cdot}25$ cm; ◇, $y = 0{\cdot}5$ cm; ▽, $y = 0{\cdot}75$ cm.

The phase velocity of the 1 Hz and 2 Hz components was determined using the method described by Stegen & Van Atta (1970) and Simmons (1974). In the present experiment the two probes were placed at a given radius in the wake. Initially the second probe was positioned 5 cm downstream of the first probe, and slightly displaced laterally to minimize interference due to the upstream sensor and its supports. The true phase difference of the two output signals (corrected to take into account the phase difference due to the relative lateral displacement of the probes) was then used to compute the appropriate wavelength and phase velocity of each component. Similar experiments were performed with streamwise separations of 2·5, 3·5 and 6·5 cm between the two probes. Only minimal variations in wavelength and phase velocity could be detected over this range of probe separations. Streamwise variation of the wavelength (λ) and phase velocity (c_{ph}) is shown for the 1 Hz component in figure 17, and for the 2 Hz component in figure 18 respectively. In each case the phase velocity has been non-dimensionalized by the free-stream velocity. Measured values of c_{ph} compare well with the theoretical values predicted by Sato & Okada. Their analysis gives $c_{ph} = 0{\cdot}84$ to $0{\cdot}9$ (depending on frequency) for the mode $n = 1$. It may be noted that λ and c_{ph} of the 1 Hz component tend to decrease initially, and then increase consistently. On the other hand, the 2 Hz component appears to maintain a nearly constant λ and c_{ph}. We also note that for this particular body at a Reynolds number of 3600,

$$\lambda_{f=1\,\mathrm{Hz}} \simeq \tfrac{1}{2} - \tfrac{2}{3} \text{ body length},$$

$$\lambda_{f=2\,\mathrm{Hz}} \simeq \tfrac{1}{4} - \tfrac{1}{3} \text{ body length}.$$

The azimuthal variation in the phase of longitudinal velocity fluctuations at various downstream locations was obtained using two probes positioned in the wake. One

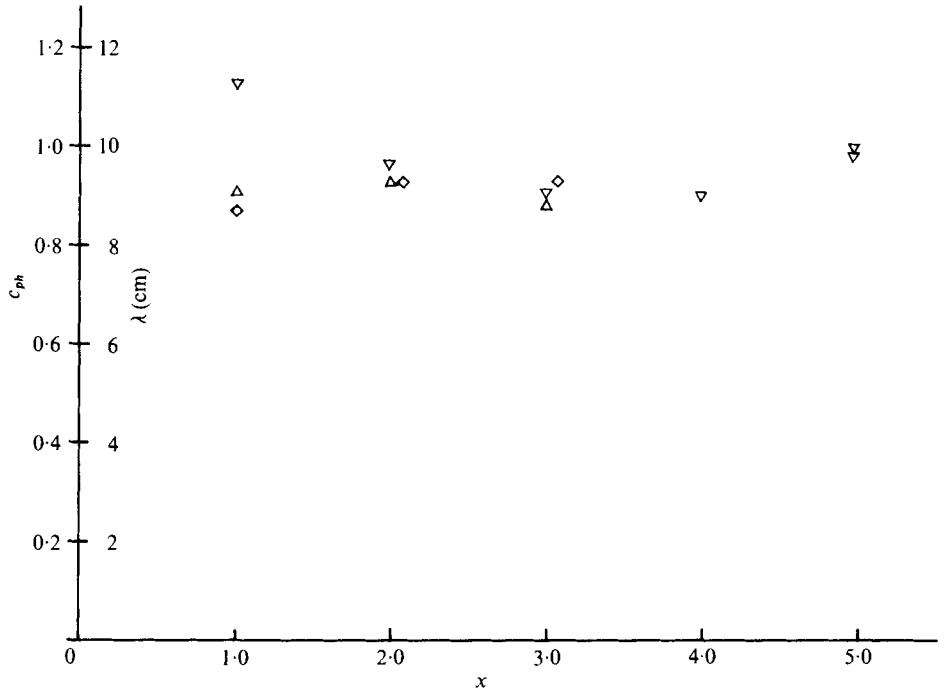

FIGURE 18. Wavelength and phase velocity of the 2·0 Hz component. For symbols see figure 17.

probe, the reference, was held at a fixed location, while a second probe was moved around a circle of radius R, centred on the wake axis, at the same x location. The radius R was selected as the radius at which peaks occurred in the bimodal amplitude distribution of the fluctuations. At various azimuthal separations ϕ, the phase difference of the signals from the two probes was computed from the digitally obtained cross-spectrum. For the 1·0 Hz component, the azimuthal variation in phase difference Θ is shown in figure 19. At $x = 0$, the phase difference shows two apparent discontinuities – changes of approximately 180° at azimuthal separations of $-60°$ and 90°–120°. Otherwise Θ does not change significantly with ϕ. In contrast, the phase difference with changing azimuthal separation is quite smooth farther downstream. Most of the data points for the entire range $x = 2{\cdot}0$ to $x = 3{\cdot}5$ fall around a line of slope $+1$, i.e. there is a one-to-one (1 : 1) correspondence between the azimuthal separation of the probes and the phase difference between the two 1·0 Hz components of the longitudinal velocity fluctuations.

These results seem to describe two different types of motion causing the 1·0 Hz disturbance, depending on the downstream location. At $x = 0$ the phase differences suggest that the velocity fluctuation at this location is a periodic side-to-side oscillation of the boundary layer on the body. At $x = 2{\cdot}5$, for example, a completely different basic motion is required to explain a phase difference which increases linearly with the azimuthal separation of the probes. Since the disturbance actually travels downstream past a given location this disturbance mode corresponds to a helix. The phase differences obtained at $x = 1{\cdot}0$ do not clearly define either a side-to-side oscillation or a

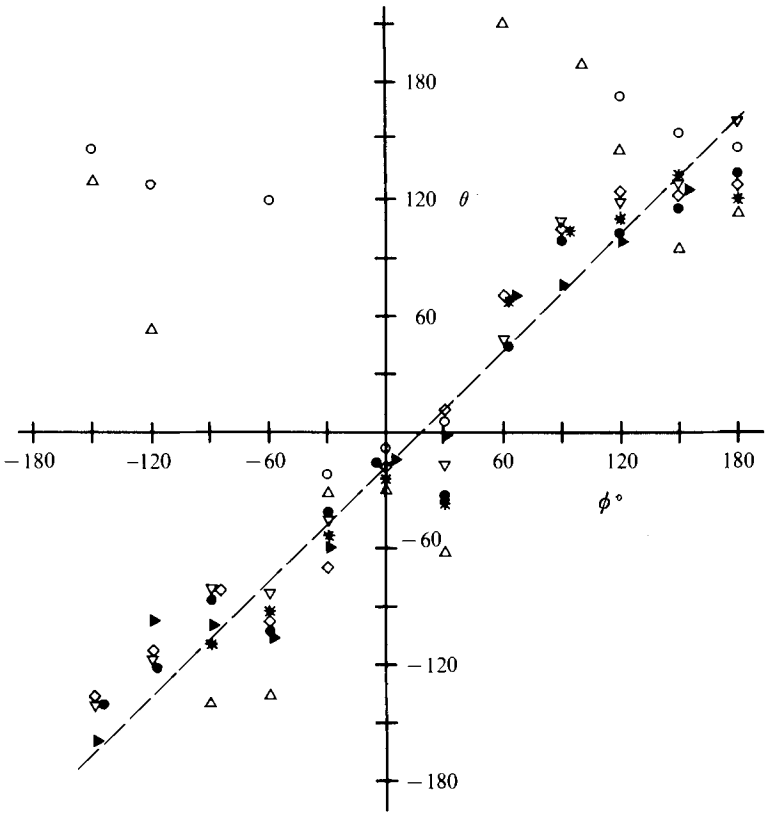

FIGURE 19. Phase difference *vs.* azimuthal separation for the 1·0 Hz component of u^*. ○, $x = 0$, $y = 0{\cdot}51$ cm; △, $x = 1{\cdot}0$, $y = 0{\cdot}51$ cm; ▽, $x = 2{\cdot}0$, $y = 0{\cdot}51$ cm; ◇, $x = 2{\cdot}5$, $y = 0{\cdot}58$ cm; ●, $x = 3{\cdot}0$, $y = 0{\cdot}58$ cm; ✱, $x = 3{\cdot}5$, $y = 0{\cdot}58$ cm; ▶, $x = 4{\cdot}0$, $y = 0{\cdot}76$ cm; – – –, line of slope +1.

helical mode, i.e. the mode of disturbance appears to be in the process of readjusting itself.

The azimuthal variation in the phase difference of the 2·0 Hz component was obtained using the same method as for 1·0 Hz and is shown in figure 20. A feature of figure 20 is that at any downstream location a phase difference of 180° occurs at azimuthal separations of approximately −30° to 0°, and also at 150° to 180°. Otherwise the phase difference changes very slowly with changes in azimuthal separation. The interpretation of these results is that the 2·0 Hz component appears to be a planar oscillatory motion. Such an oscillatory motion would generate a weak second harmonic component about an axis through the wake centre-line, orthogonal to the direction of oscillation. The azimuthal variation in amplitude of the 2·0 Hz and 4·0 Hz components in the longitudinal velocity fluctuations is shown in figure 21. The decrease in amplitude of the 2·0 Hz component, and corresponding increase in the amplitude of the 4·0 Hz component are quite definite around azimuthal separations of 150° to 180° and −30° (i.e. 330°) to 0°. These are the identical positions at which the phase of the 2·0 Hz fluctuations changed by 180°, and confirm the conclusion that the 2·0 Hz component appears predominantly as a planar oscillatory mode which it may be possible to describe in terms of a superposition of various $n = 1$

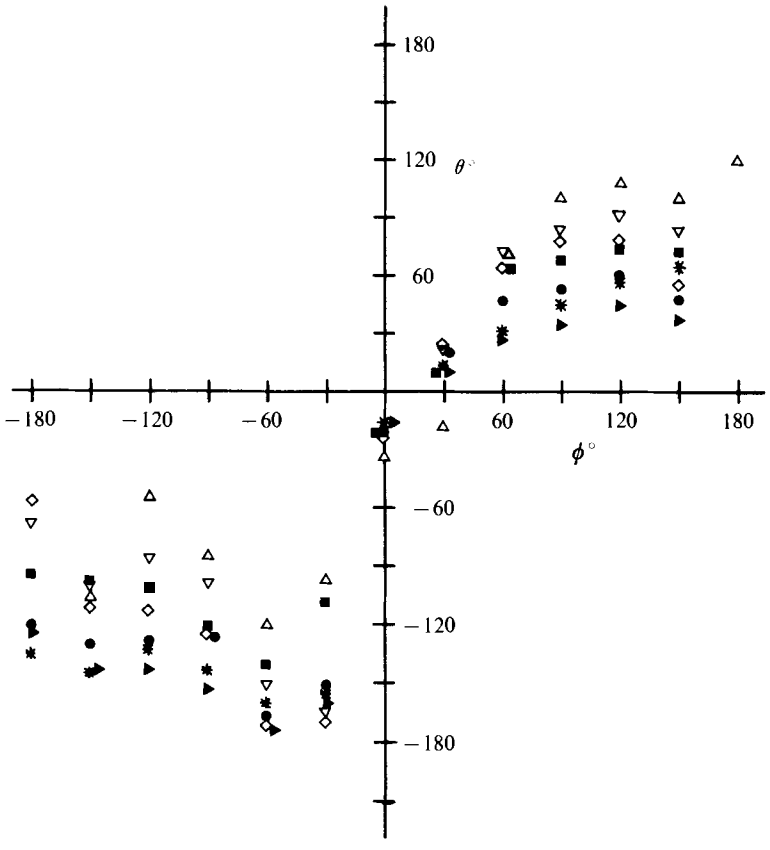

FIGURE 20. Phase difference *vs.* azimuthal separation for the 2·0 Hz component of u^*. For symbols see figure 19.

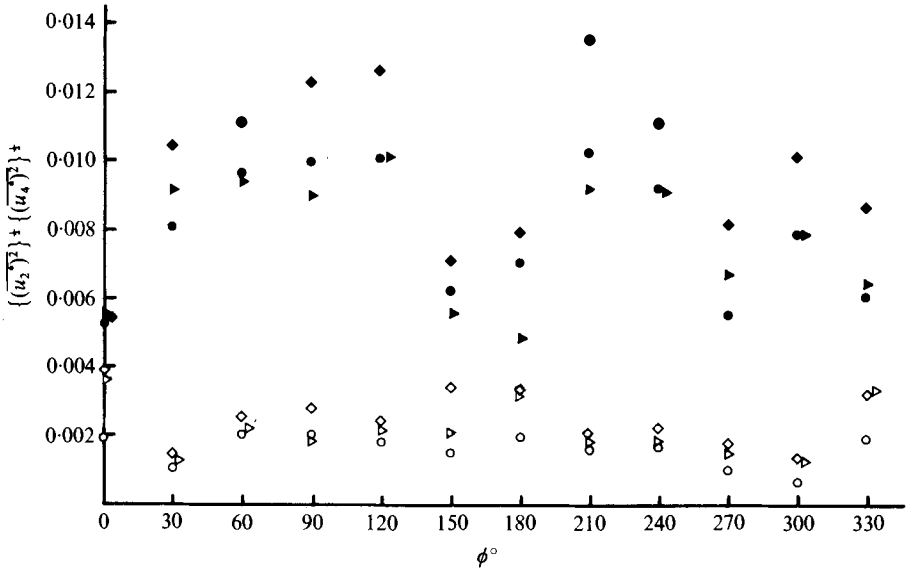

FIGURE 21. Amplitudes of the 2·0 Hz and 4·0 Hz components of u^* *vs.* azimuthal position. ●, $f = 2{\cdot}0$ Hz, $x = 3{\cdot}0$, $y = 0{\cdot}58$ cm; ◆, $f = 2{\cdot}0$ Hz, $x = 3{\cdot}5$, $y = 0{\cdot}58$ cm; ▶, $f = 2{\cdot}0$ Hz, $x = 4{\cdot}0$, $y = 0{\cdot}76$ cm; ○, $f = 4{\cdot}0$ Hz, $x = 3{\cdot}0$, $y = 0{\cdot}58$ cm; ◇, $f = 4{\cdot}0$ Hz, $x = 3{\cdot}5$, $y = 0{\cdot}58$ cm; ▷, $f = 4{\cdot}0$ Hz, $x = 4{\cdot}0$, $y = 0{\cdot}76$ cm.

modes. The generation of a weak 2·0 Hz component by the side-to-side oscillation of the boundary layer at the trailing tip of the slender body could not be verified owing to the low amplitude of fluctuations there. At $x = 0$ the 2·0 Hz component is very small, so any characteristic fluctuations would undoubtedly be masked by the higher background turbulence level.

5. Flow visualization

The hydrogen bubble technique was used to provide a visual representation of the wake. For these experiments a fine platinum wire cathode was placed perpendicular to the wake axis but inclined 45° in the azimuthal direction relative to the vertical direction, and an inclined mirror was rested on the bottom of the test section. With this configuration of inclined wire and mirror, both the side elevation and the plan view of the fine lines of bubbles were visible simultaneously when the arrangement was viewed from the side.

Figure 22 (plate 2) is a photograph of the flow regime previously identified as the region of locally parallel flow. The left-hand edge of the photograph is at about $x = 1{\cdot}6$, and the right-hand edge is at $x = 2{\cdot}75$. Flow is from left to right, and the scale is in inches. The upper portion of the photograph is the side elevation of the lines of bubbles generated by pulsing the oblique wire. Since the wire is vertical from this point of view, the lines of bubbles also appear to be vertical. The lower part of the photograph is the reflexion of the lines of bubbles in the inclined mirror. The distance between successive crests or troughs of the wave pattern in the upper portion of the photograph is approximately three inches, or 7·6 centimetres. This distance compares well with the wavelength of approximately 8·0 cm for the 2·0 Hz component obtained from the phase speed measurements. As was shown earlier, the amplitude of the 2·0 Hz component is significantly larger than that of the 1·0 Hz component in this downstream region. This would account for the apparent masking of the 1·0 Hz helical mode in this photograph.

The instantaneous velocity profile is seen to be skewed away from the symmetrical mean profile in both the side elevation and plan view of the wake. This variation is most apparent in the vicinity of the wake axis, although some waviness is apparent near the free stream.

An observation from figure 22 is that the oscillatory wave pattern in the wake becomes asymmetrical. In the side elevation, down to about 4 on the scale, the deformation is the same on both sides of the axis. Further downstream, displacements towards the scale, i.e. the troughs in the wave pattern, such as at 5, 8 and 10·75 on the scale, are sharper than the crests away from the scale. It appears that the wave pattern in the plan view does not show the same excessive distortion or skewness of the velocity profile as in the side elevation. A hasty conclusion should not be drawn from these limited observations, however, since some of these patterns might have resulted from a particular orientation of the bubble-producing wire.

A second photograph, covering the downstream region $x = 2{\cdot}5$ to $x = 3{\cdot}75$, is shown in figure 23 (plate 3). Although the frequency at which the bubble-generating wire was pulsed has been increased for this photograph, the configuration of oblique wire and inclined mirror is the same as previously described. At the left-hand edge of the

photograph, the waviness characteristic of the nearly parallel flow regime can be seen. At about the position 6 on the scale, a distinctive change in the nature of the waviness is occurring. The plan view shows that there is an abrupt shift of the lines of hydrogen bubbles towards the scale. Farther downstream large-scale transverse fluctuations with a definite longitudinal spacing have formed. It is significant that the transverse motion is most apparent in the upper portion of the photograph (the side elevation) whereas the lower portion shows what appear to be tangled lines of hydrogen bubbles.

The large-scale disturbances have a streamwise spacing approximately the same as the spacing of the sharp troughs of the higher frequency mode in the nearly parallel flow regime. Careful examination of this photograph shows that between 9·5 and 10·5, and 12 to 13 (approximately) on the scale, the lines of hydrogen bubbles appear to be rolling up on themselves. It is possible that this is associated with a three-dimensional vortex filament of some sort. Hama (1963) has shown that a curved vortex filament undergoes further deformation as a result of its own induced velocity field. As time elapses, the vertex of the vortex filament rises away from the plane in which it was initially formed. Owing to the three-dimensional structure the vortex filaments acquire in the axisymmetric wake, they will undergo a similar self-induced motion in the radial direction (away from the axis). This mechanism could account for the appearance of disturbances with the large radial displacements and the roll-up of fluid in the wake as shown in figure 23.

Studies of the hydrogen bubbles over an extensive period of time showed that these large-scale structures did not always form at exactly the same downstream location. Instead, their formation was observed to be a seemingly random and intermittent occurrence anywhere between $x = 3{\cdot}0$ and $x = 4{\cdot}5$. Previously it was remarked that the signals near the outer edge of the wake in the far downstream region show frequent large downward spikes in a signal otherwise devoid of large fluctuations. These spikes were interpreted as sudden decreases in the mean velocity. A hot-film sensor placed well away from the axis at a far downstream position, such as 13 on the scale in figure 23, will encounter occasional patches of lower momentum fluid as a result of the retarding effect of the three-dimensional vortex structures. As each vortex moves past the sensor, the sensor experiences a momentary decrease in the mean velocity of the fluid, thereby producing a downward spike in its output signal.

The variation in the downstream position at which these large-scale structures develop is a result of the randomness associated with the natural transition. The actual nature of the vortex filaments, i.e. their three-dimensional structure and development, is unknown at this time.

6. Discussion

During the course of these experiments it became apparent that the alignment of the slender body was of critical importance in obtaining an axisymmetric wake. Misalignment by as little as one minute of arc was sufficient to cause noticeable asymmetry in the mean velocity profile of the wake, and at the same time cause the wake to become turbulent much closer to the trailing tip of the body. Once the body was well aligned in the test section, the breakup of the dye trace shown in figure 1 always occurred in the downstream region $x = 3{\cdot}5$ to $x = 5{\cdot}0$. Interpretation of the

data from the natural transition experiment with an axisymmetric wake is considerably more difficult than the case of transition induced by artificial stimulation of particular disturbance modes.

Our experiments suggest that the axisymmetric wake which undergoes natural transition can be divided into three distinct regions.

(*a*) *The adjustment region, or near wake*

The adjustment region exists from the trailing tip of the body $x = 0{\cdot}0$ to about $x = 1{\cdot}5$. This region is formed as the boundary layer swept off the slender body adapts itself to the conditions of the free shear layer forming the wake. The region is characterized by large gradients in the mean velocity field in both the radial and the streamwise direction. The mean-velocity profile of the boundary layer changes to the wake profile, which is approximately the same as the mean profile predicted by an asymptotic similarity theory. This theory is developed assuming very small velocity defects compared with the free-stream velocity, however, the mean velocity profile becomes self-similar even when the centre-line velocity defect is still sizable.

Within this region the disturbances present in the boundary layer of the body appear to adjust themselves to disturbances in the wake. The radial variation in the amplitude of the longitudinal velocity fluctuations is bimodal, with an extremely small value on the wake axis. Measurements of phase differences between longitudinal fluctuations at $x = 0{\cdot}0$ suggest that the disturbance in the boundary layer is a side-to-side oscillation. On the other hand, at $x = 1{\cdot}5$ the dominant fluctuation appears to be helical in structure. The mechanism of selection and transformation from one mode to another is not completely understood. The background turbulence is large compared with the amplitude of the principal 1·0 Hz component, and tends to randomize the latter. As a consequence, none of the fluctuations has a uniformly regular structure that can be identified at any given instant of time.

(*b*) *The region of locally parallel flow*

The locally parallel flow regime exists from about $x = 1{\cdot}0$ to $x = 3{\cdot}0$. In this region the mean velocity profile is self-similar and the centre-line velocity and the half-value radius increase relatively slowly with the downstream distance.

The radial distribution of the amplitude of the longitudinal velocity fluctuations remains bimodal in form, with a small amplitude on the wake axis. The actual velocity fluctuations are regular in frequency, and appear to be amplitude modulated to some extent. Spectral analysis of the velocity fluctuations shows that two distinct frequency components are present in the signals. A well defined 1·0 Hz component present in the signals at $x = 1{\cdot}5$ is overwhelmed by a component of about 2·0 Hz farther downstream. Both components show a bimodal amplitude distribution in the radial direction, with low amplitude fluctuations on the wake axis. The amplitudes of both components increase exponentially with downstream distance and detailed phase measurements suggest that the 1·0 Hz disturbance is helical in structure, whereas the 2·0 Hz disturbance with higher amplification rate appears to be predominantly a planar oscillation.

The experimentally determined spatial amplification rates of the 1·0 Hz and 2·0 Hz components were converted to effective temporal amplification rates using Gaster's (1962) transformation, and are shown, together with the neutral stability curves of

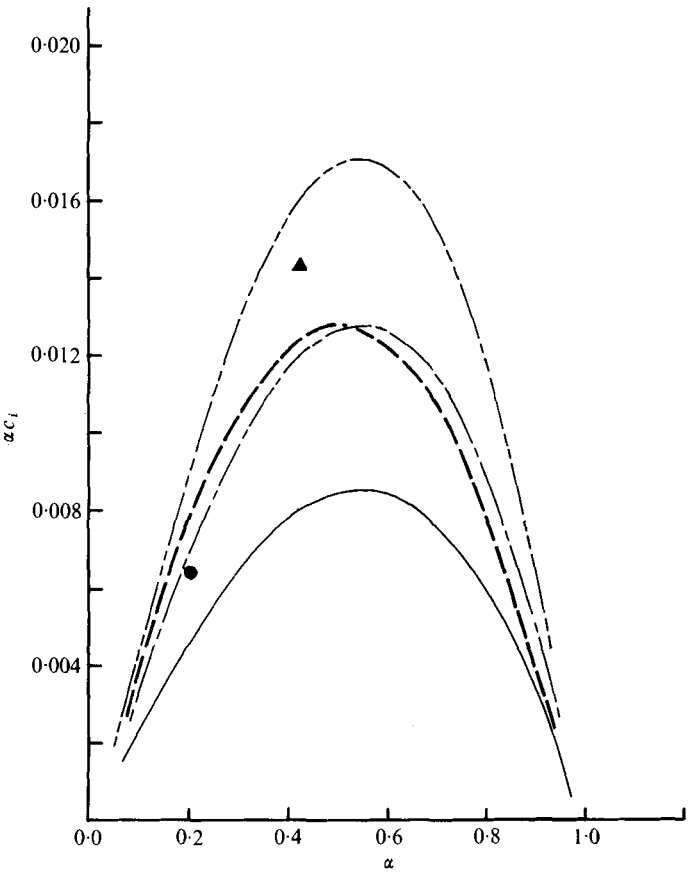

FIGURE 24. Temporal amplification rate *vs.* non-dimensional wavenumber for the linear inviscid stability theory, showing (*a*) – – –, Sato & Okada; (*b*) Lessen & Singh, ——, $u_c = 0{\cdot}2$; — · —, $u_c = 0{\cdot}3$; — · · —, $u_c = 0{\cdot}4$; (*c*) present experimental results; ●, $f = 1{\cdot}0$ Hz, $0{\cdot}35 < u_c < 0{\cdot}7$, $\alpha = 0{\cdot}214$, $(\alpha c_i) = 0{\cdot}00683$; ▲, $f = 2{\cdot}0$ Hz, $0{\cdot}35 < u_c < 0{\cdot}7$, $\alpha = 0{\cdot}429$, $(\alpha c_i) = 0{\cdot}0143$.

the inviscid temporal stability theories, in figure 24. The temporal amplification rates are

(*a*) for the 1·0 Hz component: $(\alpha c_i) = 0{\cdot}00683$,

(*b*) for the 2·0 Hz component: $(\alpha c_i) = 0{\cdot}0143$.

Figure 24 shows that the non-dimensional wavenumber for the 2 Hz disturbance we identify is near that at which maximum amplification occurs according to the linearized inviscid theory of the stability of the $n = 1$ mode. Moreover, the temporal amplification rate we obtain for this disturbance is comparable to theoretical values for the $n = 1$ mode calculated using centre-line velocity defects measured in this region of locally parallel flow, although the simple $n = 1$ mode at this frequency could not be identified unambiguously.

(*c*) *The far wake*

The first quantitative indication that the nature of the wake changes far downstream comes from the measurements of half-value radius and centre-line velocity. Downstream of $x = 3{\cdot}5$, both of these characteristics of the mean velocity profile increase

somewhat more rapidly than in the region of locally parallel flow. Identification of the laminar–turbulent transition on the basis of the mean-flow characteristics is difficult in the axisymmetric wake. In contrast to boundary-layer transition, neither the spreading rate, the centre-line velocity increase nor the mean velocity profile is significantly distinguishable between laminar and turbulent conditions.

In addition to these changes in the mean profiles, the velocity fluctuations take on a different profile. On the wake axis bursts of large amplitude fluctuations appear in an otherwise quiescent signal. These bursts are composed only of positive velocity fluctuations, and no negative fluctuations have been observed at this location. Large increases in the overall r.m.s. amplitude of the signal and the amplitudes of the 1·0 and 2·0 Hz components accompany the appearance of these bursts. The bimodal amplitude distribution observed near the body no longer appears as the maximum amplitude of the fluctuations develops on the wake axis. At $x = 4{\cdot}0$ and 5·0, velocity fluctuations on the axis have the appearance of a 'turbulence-like' signal. With the production of mostly random velocity fluctuations, the energy spectra become smoother and devoid of distinct peaks.

Away from the wake axis the regular signals of the locally parallel flow region are interspersed with bursts of apparently random fluctuations. Both positive and negative peaks are observed here, in contrast to the positive-only peaks on the wake axis. As the downstream distance is increased, the proportion of random fluctuations in the signals increases, and the amplification rates of particular components become very small. These factors indicate that the regular disturbances are breaking down and the flow is becoming turbulent.

An interesting observation is that the random bursts appear to form first on the wake axis and then spread outwards until the entire wake is turbulent.

7. Summary

This study of the axisymmetric wake behind a slender streamlined body indicates that in a natural transition experiment the wake may be classified into three regions. As the distance from the trailing tip of the body increases, these regions are:

(*a*) the adjustment region; (*b*) the region of locally parallel flow, (*c*) the far wake.

In the adjustment region the boundary layer of the slender body adapts itself to the conditions of the wake. The adjustment is accompanied by changes in the mean velocity profile, and in the nature of the disturbances in the flow. Initially the disturbance appears to be very small side-to-side fluctuations in the boundary layer of the generating body, but further downstream a low frequency helical disturbance develops.

The locally parallel flow region is identified by a mean velocity distribution that undergoes very slow changes as the downstream distance increases. Spectral analysis of the velocity fluctuations in this region show that at least two distinct components are present, each with its own frequency, amplification rate, phase velocity and structure. There does not appear to be any interaction of these two components. The amplitudes of both components increase exponentially with downstream distance and the non-dimensional wavenumber of the apparent higher frequency mode is very close to that at which maximum amplification occurs according to the linear inviscid stability theory.

In the far wake, bursts of random fluctuations appear in a signal otherwise com-

posed of regular fluctuations. In hydrogen bubble photographs of this region, large-scale transverse structures which may be associated with the formation of a discrete vortex array have been observed. The initial streamwise spacing of these structures is apparently related to the wavelength of the oscillatory disturbance observed in the region of locally parallel flow. The appearance of random fluctuations and the eventual breakdown of the regular fluctuations into turbulence is believed to be intimately related to the formation of these large-scale disturbances.

The detailed process of natural transition of an axisymmetric wake is by no means fully understood. In the adjustment region, the mechanism of selection of one mode of disturbance over another mode remains a mystery. Any experimental attempt to verify a hypothesis for this changeover would be extremely difficult owing to the random nature of the very small velocity fluctuations in the region in which the transformation takes place. This randomness would have the effect of 'diluting' the fluctuations to a level so low that the physical structure of characteristic disturbances is not clearly definable. In the far wake region the actual structure of the large-scale transverse disturbances, and the manner in which the turbulent wake is established, can only be conjectured in the broadest possible terms at this time.

The authors wish to express their gratitude to their colleagues at Princeton University for their advice and support, and acknowledge their indebtedness to Dr G. R. Stegen for his assistance with the digital analysis of the experimental data. The continued sponsorship of this research by the National Science Foundation through grants GK-20409 and ENG 74-21490 is also gratefully acknowledged.

REFERENCES

BATCHELOR, G. K. & GILL, A. E. 1962 *J. Fluid Mech.* **14**, 529–551.

CHEVRAY, R. 1968 *J. Basic Engng, Trans. A.S.M.E.* D **90**, 275–284.

CURLE, N. 1957 *Proc. Roy. Soc.* A **238**, 489–501.

FREYMUTH, P. 1966 *J. Fluid Mech.* **25**, 683–704.

GASTER, M. 1962 *J. Fluid Mech.* **14**, 222–224.

HAMA, F. R. 1963 *Phys. Fluids* **6**, 526–534.

HAMA, F. R. & PETERSON, L. F. 1976 *J. Fluid Mech.* **76**, 1–15.

KENDALL, J. M. 1975 *A.I.A.A. J.* **13**, 290–299.

LAUFER, J. & VREBALOVICH, T. 1960 *J. Fluid Mech.* **9**, 257–299.

LESSEN, M. & SINGH, P. J. 1973 *J. Fluid Mech.* **60**, 433–457.

LIN, C. C. 1944–1945 Parts 1, 2, 3 of *Quart. Appl. Math.* pp. 117–142, 218–314, 277–301.

MACK, L. M. 1969 Boundary-layer stability theory. *JPL Rep.* 900-277 *Rev. A.*

MATTINGLY, G. E. & CHANG, C. C. 1974 *J. Fluid Mech.* **65**, 541–560.

MATTINGLY, G. E. & CRIMINALE, W. O. 1972 *J. Fluid Mech.* **51**, 233–272.

MICHALKE, A. 1965 *J. Fluid Mech.* **23**, 521–544.

MORRIS, P. J. 1976 *J. Fluid Mech.* **77**, 511–529.

PETERSON, L. F. 1975 Ph.D. thesis, Department of Aerospace and Mechanical Sciences, Princeton University.

REYNOLDS, A. J. 1962 *J. Fluid Mech.* **14**, 552–556.

ROSENHEAD, L. 1963 *Laminar Boundary Layers.* Oxford University Press.

SATO, H. 1959 *J. Fluid Mech.* **7**, 53–80.

SATO, H. & KURIKI, K. 1961 *J. Fluid Mech.* **11**, 321–352.

SATO, H. & OKADA, O. 1966 *J. Fluid Mech.* **26**, 237–253.

SATO, H. & SAITO, H. 1975 *J. Fluid Mech.* **67**, 539–559.

SCHUBAUER, G. B. & SKRAMSTAD, H. K. 1947 *N.A.C.A. Rep.* 909. (See also *J. Res. Nat. Bur. Stand.* **38**, 257–292.)

SIMMONS, J. E. L. 1974 *J. Fluid Mech.* **64**, 599–609.

STEGEN, G. R. & VAN ATTA, C. W. 1970 *J. Fluid Mech.* **42**, 689–699.

TATSUMI, T. & KAKUTANI, K. 1958 *J. Fluid Mech.* **4**, 261–275.

VIILU, A. 1962 *J. Appl. Mech.* **29**, 506–509.

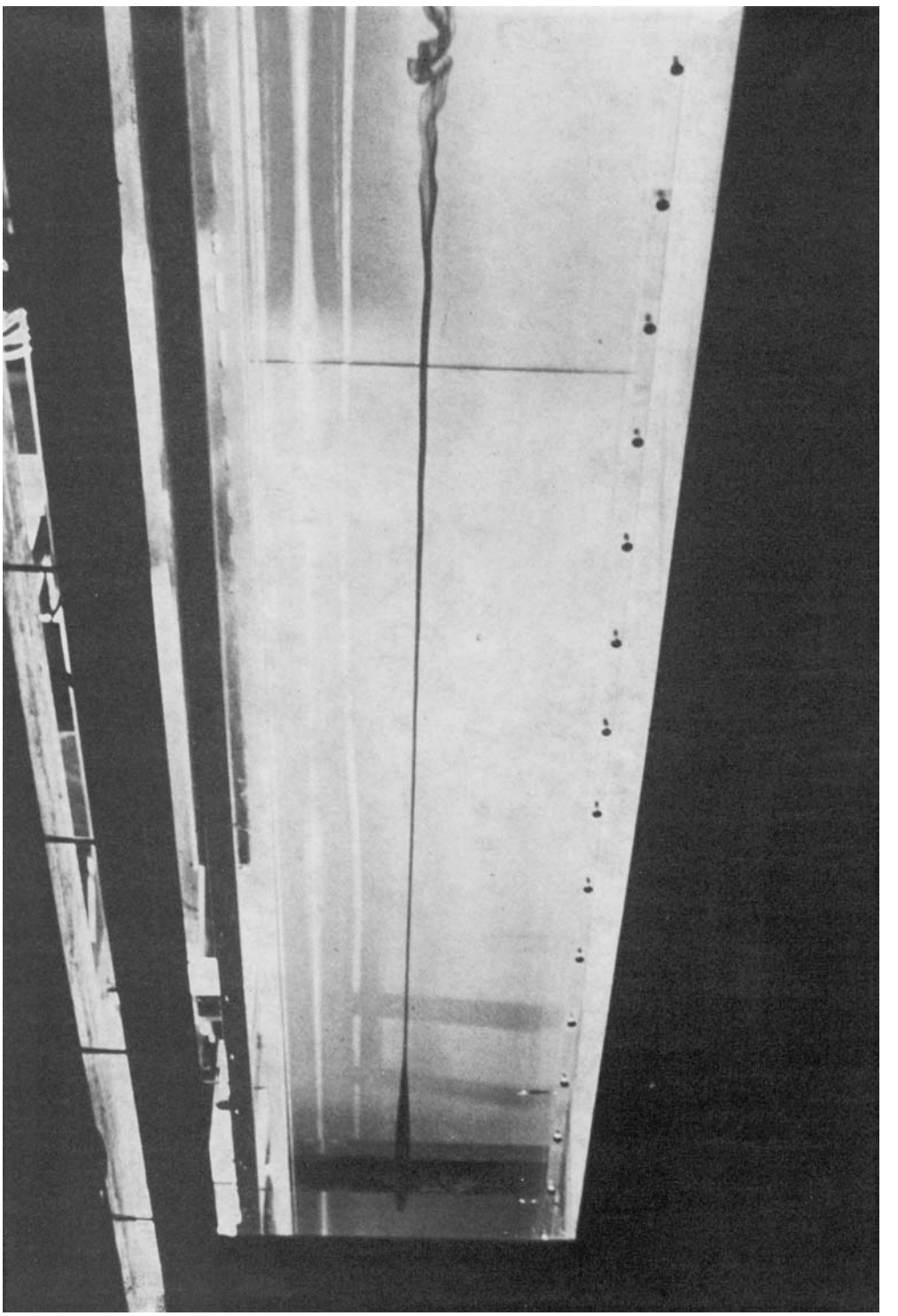

FIGURE 1. Photograph of the slender body suspended in the test section of the flume. Water flow is from left to right. Trypan blue dye streak indicates the inner core of the wake. $R = U_0 d/\nu = 3600$.

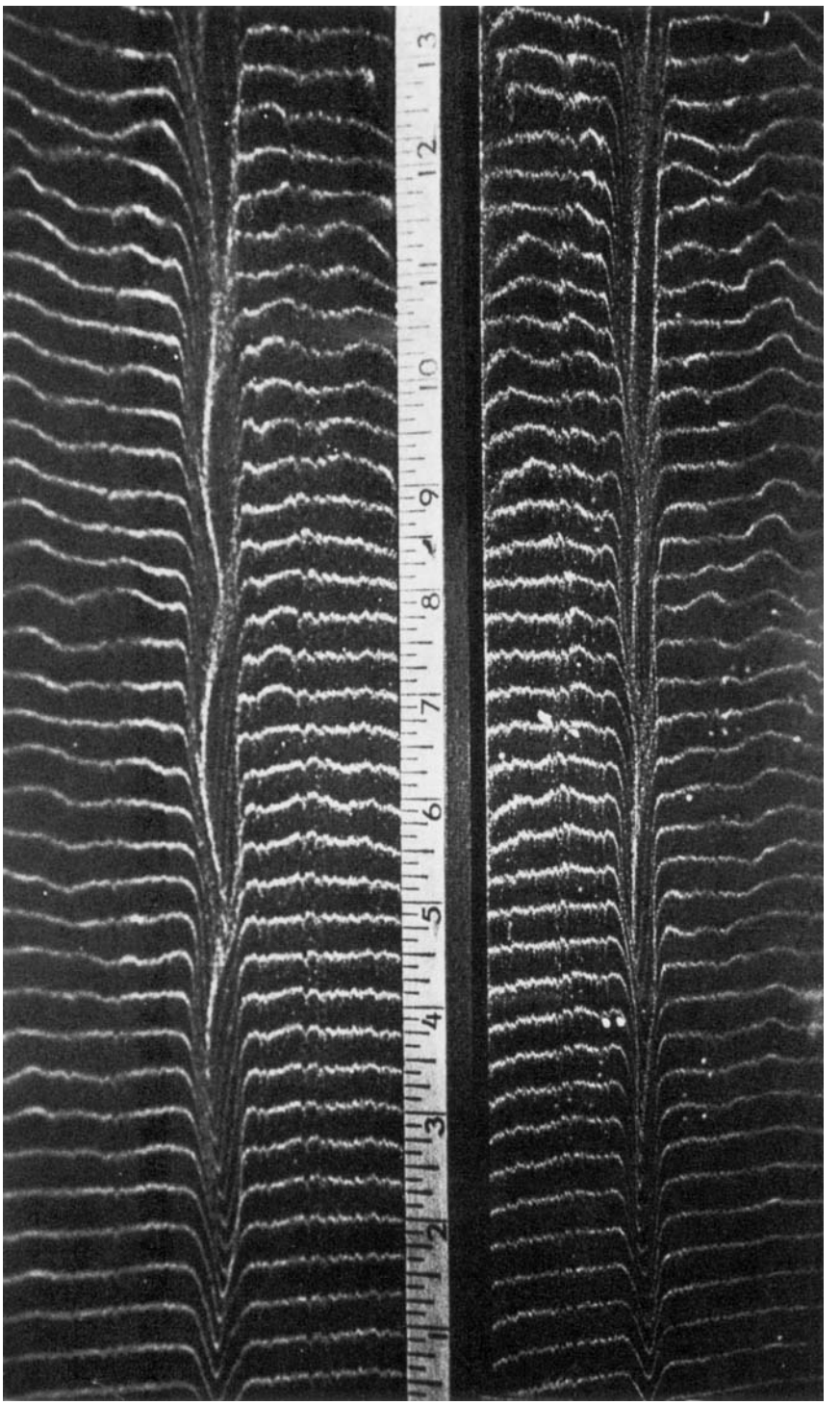

FIGURE 22. Hydrogen bubble photograph of the region in which locally parallel flow exists. $x = 1{\cdot}6$ to $x = 2{\cdot}75$. Flow is from left to right, scale is in inches.

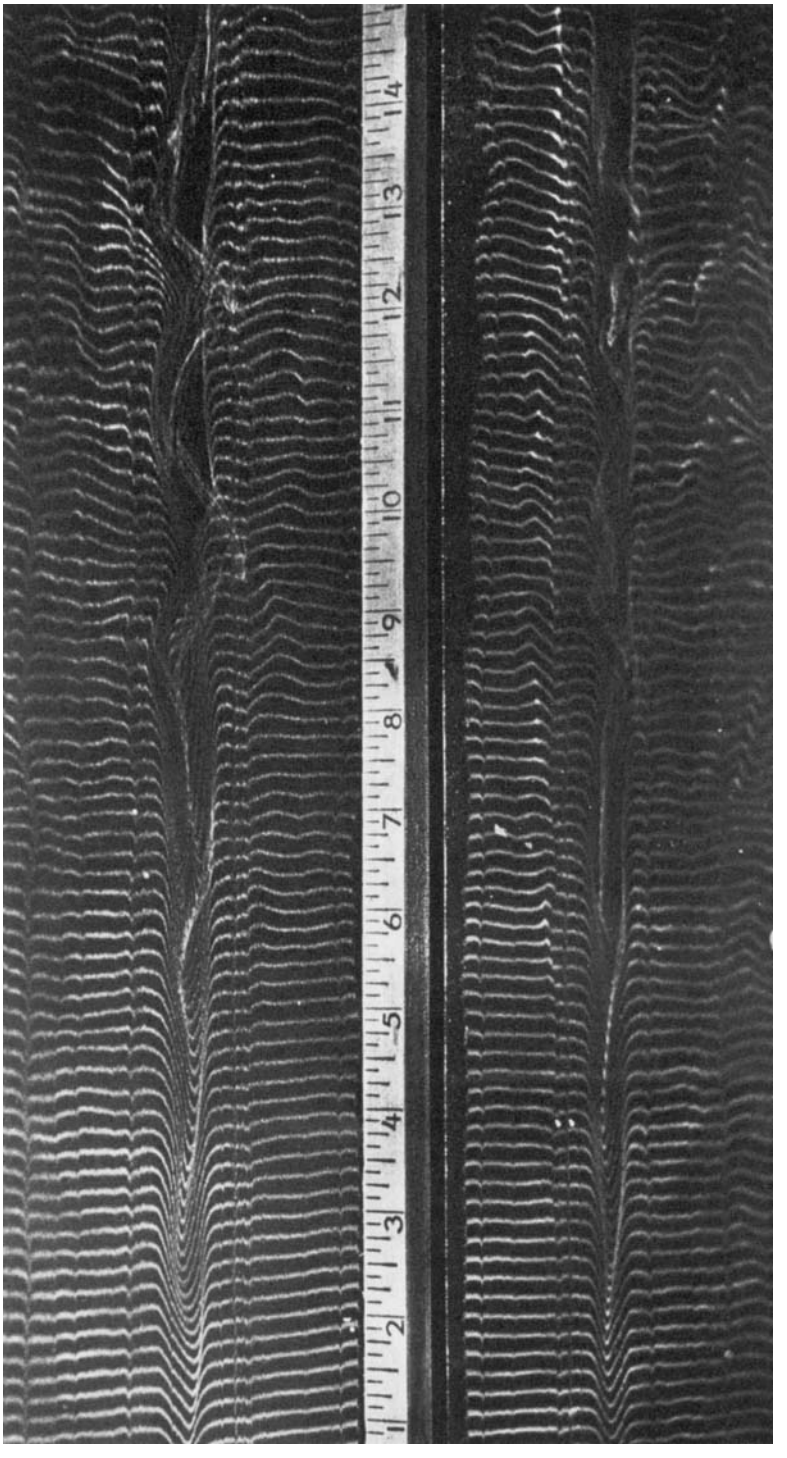

FIGURE 23. Photograph of hydrogen bubbles in the flow region $x = 2{\cdot}5$ to $x = 3{\cdot}75$. Flow is from left to right, scale is in inches.